Progress in Medical Devices
ISSN: 2957-5478

Zentime

Research Article https://doi.org/10.61189/063815kuibzu

Design and verification of the testing device for thoracic aortic stent grafts

Yu Zhou[1], Shiju Yan[1], Ailing Zhang[2]

[1]School of Health Science and Engineering, University of Shanghai for Science and Technology, Shanghai 200082, China. [2]College of Health Management, Shanghai Jian Qiao University, Shanghai 201306, China.

Corresponding author: Ailing Zhang.

Declaration of conflict of interest: None.

Received January 22, 2025; Accepted March 13, 2025; Published September 30, 2025

Highlights

- A novel testing device for measuring the radial support force and bending spring-back force of stent grafts has been developed.
- A theoretical geometric model for the bending behavior of stent grafts was derived and applied in numerical simulations, significantly enhancing the simulation results.
- The device's reliability was validated by comparing numerical simulation outcomes with physical experimental results under varying compression diameters and bending angles.

Abstract

Objective: To design a testing device for measuring the radial support force and bending spring back force of stent grafts and evaluate its effectiveness. **Methods:** A radial force and spring-back force testing device was designed to integrate with a tensile testing machine. The radial compression and bending characteristics of stent grafts for thoracic aorta applications were analyzed, and the corresponding conversion formulas were derived. A custom stent ring fixture was fabricated, and a five-wave gradient stent was sewn. Both physical experiments and finite element simulations were conducted. Radial support forces were measured by gripping 20%, 40%, and 60% of the stent's diameter, and bending tests were performed at angles of 60°, 90°, and 180°. The stability of the testing device was analyzed through comparative tests across different compression diameters and bending angles. **Results:** The device demonstrated high detection precision, stability, and accuracy, with minimal deviation across multiple measurements. The mechanical behavior of the stent observed in both finite element simulations and physical experiments showed consistent results. **Conclusions:** The testing device developed in this study effectively measures the mechanical changes in large-diameter stent grafts, providing a new reference for testing large-diameter stents.

Keywords: Stent grafts, testing device, bending spring back force, radial support force

I Introduction

Since Dake et al. first successfully applied thoracic endovascular aortic repair (TEVAR) to treat thoracic aortic aneurysms, the technique has continuously evolved [1]. Currently, large-diameter self-expanding stents are commonly used for treating such conditions. Once implanted, these stents effectively expand the vessel and block abnormal blood flow. In addition to biocompatibility, the mechanical properties of stent grafts is closley associated with the effectiveness of TEVAR and the occurrence of postoperative complications [2].

Radial support force and spring-back force are key indicators for evaluating the mechanical performance of stents [3-5]. Insufficient radial support force can result in poor fixation of the stent graft within the vessel, leading to displacement or endoleaks due to blood flow [6]. Conversely, excessive radial support force may damage the vessel intima [7]. Spring-back force refers to the inherent tendency of self-expanding endografts to return to their original shape when passively bent, such as when positioned across the aortic arch [8]. When spring-back force is too high, the stent graft's apposition

Address correspondence to: Ailing Zhang, College of Health Management, Shanghai Jian Qiao University, NO. 1111 Hucheng Ring Road, Pudong New Area, Shanghai 201306, China, Tel: +86-18616022898. E-mail: zhangailing@gench.edu.cn.

to the vessel wall is compromised, potentially causing the "bird beak phenomenon" and endoleaks [9]. Moreover, excessive stress at the contact points between the stent and the vessel wall can lead to intimal tearing, resulting in the formation of new entry tears [10, 11]. To address these issues, prior studies have focused on enhancing stent support and compliance through modifications in stent materials, peak designs, or by adding connecting struts [12-14]. However, assessing the effectiveness of these modifications requires the development of reliable and scientific testing devices.

Radial support force is commonly measured using methods such as planar compression, V-groove compression, and iris rolling compression [15]. In planar compression, parallel pressing plates are moved vertically to compress the stent, yielding a single radial support force value, but its reference value is limited [16, 17]. The V-groove compression method improves upon planar compression, by subjecting the stent to three-directional forces during compression [18-20]. However, different stent outer diameters require corresponding V-groove sizes, limiting the equipment's applicability. The iris rolling compression method applies radial compression using fan-shaped blocks arranged circumferentially. As the number of fan-shaped blocks increases, the contact surface approximates a circular shape, providing a more accurate reflection of the stent's radial support performance [21]. However, the complex structure of the equipment makes it difficult to avoid interference and friction among various mechanisms during production, resulting in high manufacturing and processing difficulty.

Methods such as cantilever beam bending, three-point bending, and four-point bending are commonly used to measure the spring-back force of stents. In the cantilever beam method, one end of the stent is fixed, and deformation force is applied to the other end, causing the stent to bend [20]. This method avoids the influence of stent movement on the spring-back force test and allows for continuous measurement at different angles. However, the direction of the dynamometer may not be perpendicular to the testing interface, and the result is a component force. In 2000, Ormiston et al. suspended a vascular stent with a steel hook and conducted a three-point bending experiment [22]. While the loading method was simple, it caused uneven bending of the stent. The four-point bending method places the sample on two loading points and applies pressure on two points above them, ensuring even distribution of the bending moment and yielding more accurate results [23]. However, its complex structure limits its application.

The thoracic aortic stent graft, a type of large vascular stent, poses significant challenges in measuring its radial mechanical properties due to its cylindrical structure. During bending, the spring-back force of the stent changes continuously along the vertical direction of the bending arc, making accurate measurement difficult. Based on these two key characteristics and current advances in radial support force and spring-back force detection, this study proposes a new testing device that is simple to manufacture and can be used in conjunction with a tensile testing machine. The feasibility of this device is verified through physical experiments and finite element simulations, and the reliability of the test results is analyzed.

II Materials and methods

Conversion formulas

The testing device for the stent graft is used in conjunction with the tensile testing machine. Through this device, the tensile force from the tensile testing machine is converted into radial compression and bending forces for the stent graft. This allows for the precise force measurement system of the tensile testing machine to be utilized for detecting the radial support force and spring-back force of the stent.

Compression of the stent graft requires the application of circumferential pressure. By winding silk threads around the stent and applying tensile force, the tensile force is converted into circumferential pressure, causing the ring of the stent graft to compress [24]. The relationship between the radial force from the silk threads and the circumferential tension borne by the stent is given by:

$$F_R = 2\pi F_{circle} \tag{1}$$

where F_R represents the radial support force, and F_{circle} represents the circumferential tension. Since the tensile force F_l of the tensile testing machine in this experiment is twice that of F_{circle}, the relationship between the radial force and the tensile force measured by the tensile testing machine is:

$$F_R = \pi F_l \tag{2}$$

The model of the testing device for the spring back force is shown in **Figure 1**. By applying tensile forces at both ends, the stent graft is made to bend. Assuming that the target bending angle of the stent graft is α, the stent reach-

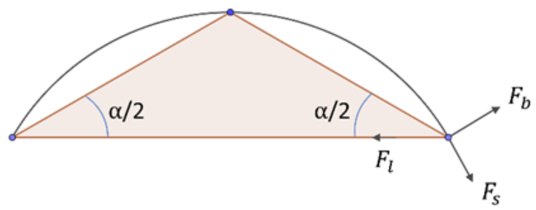

Figure 1. Mechanical model of the spring back force detection device.

es this angle when one end of it is bent by α/2. Let F_l be the tensile force at one end of the stent, F_s be the axial support force along the stent, and F_b be the spring-back force perpendicular to the axial direction of the stent. From this, the relationship between the spring back force and the tensile force can be derived as follows:

$$F_b = \frac{F_l}{sin\alpha} \tag{3}$$

Fabrication

As shown in **Figure 2A**, the compression device consists of an aluminum alloy support frame, black sliding rails, black sliders, stainless steel fixed pulleys, nylon threads, and white stent sleeves. The support frame provides overall stability. The sleeves are used to fix the two ends of the stent graft, while the sliders are employed to position and secure the sleeves. Four small metal pulleys are mounted on the support frame. Two pulleys are positioned on either side of the tensile axis of the tensile testing machine to ensure that the tensile force is transmitted vertically downward through the threads. The other two pulleys are aligned parallel to the top surface of the stent graft, ensuring that the force is applied horizontally along the tangent of the stent after being transmitted. The magnitude of the radial support force can then be accurately calculated using Equation (2).

As shown in **Figure 2B**, the bending and spring-back force testing device retains rotational and axial translational freedom when the two ends of the stent are bent. Compared to the radial compression device, this device replaces the aluminum alloy support frame and adjusts the positions of the two metal pulleys. White pulleys are installed on the two sliders to allow for the release of rotational freedom. The positions of the pulleys along the tensile axis of the tensile testing machine remain unchanged. Two metal pulleys are installed in parallel on the bottom surfaces of the sliders through angled stents. The thread on the left pulley is fixed to the right slider, and the installation method for the thread on the other side is the same. This configuration allows the two sliders to move inward as the threads are stretched horizontally, thereby bending the stent graft.

Physical experiments

Fabrication of the stent graft samples

A five-peak, Z-shaped, gradually varying stent graft was used in this experiment, as shown in **Figure 3A** [25]. The stent ring has a diameter of 33 mm, with a total length of 130 mm. Based on commercially available stents, the selected design includes seven stent rings with peak heights ranging from 10 mm to 16 mm. Other parameters include a stent wire diameter of 0.5 mm, a ring spacing of 18 mm, a coating film thickness of 0.1 mm, and a fillet radius of 0.5 mm at the peak.

Since each ring in the Z-shaped stent graft is identical, only a single-ring mold is required. As shown in **Figure 3D**, the mold is a hollow cylindrical structure with an outer diameter of φ= 33 mm [26]. Positioning holes corresponding to the fillets at the ring peaks are drilled into the mold, and adjustable pins are installed. After winding the stent wire around the pins, a pre-formed ring is shaped, and its ends are joined and fixed. Finally, the ring is sewn onto the coating film to assemble the complete stent graft.

Experimental platform and setup

The experimental platform utilizes the INSTRON 5965 dual-column tabletop electronic universal testing machine, which provides high-precision load measurements with an accuracy of±0.5% of the indicated value.

Physical experiment on radial compression

The radial support force was tested using the previously fabricated five-peak stent graft and the setup illustrated in **Figure 2A**. This device converts the tensile force generated by the testing machine into circumferential pressure applied to the stent, inducing ring compression. The machine simultaneously records displacement and force output at the terminal.

Compression displacements were incrementally increased to 20%, 40%, and 60% of the original stent diameter. Let D_0 be the original diameter, Dn the target diameter, and X the tensile displacement. According to the following formula:

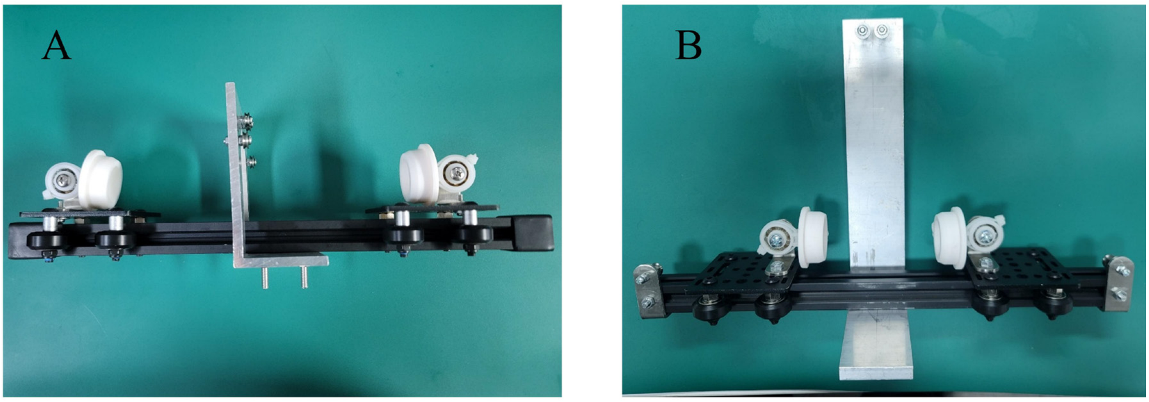

Figure 2. Physical mechanical testing device. (A) Radial support force testing device; (B) Spring back force testing device.

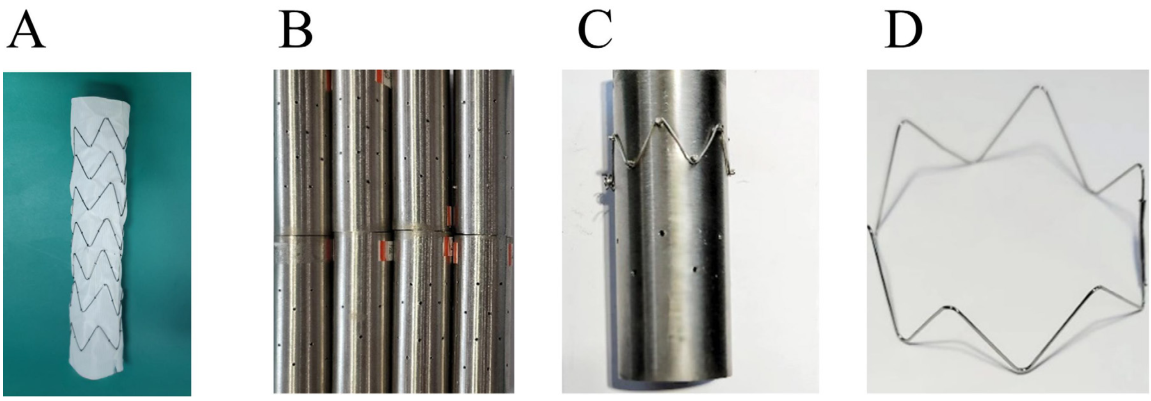

Figure 3. Mold and process for stent graft production. (A) Stent ring production mold set; (B) Support ring processing; (C) Stent ring; (D) Stent graft.

$$2*X=\pi*Do - \pi*Dn \tag{4}$$

The corresponding parameter changes are shown in **Table 1**.

During testing, all threads must remain in the same plane, and slippage at the pulleys must be avoided to ensure measurement accuracy. The tensile testing machine continuously monitors tensile force and thread displacement in real time, outputting data accordingly. The recorded tensile force is converted into radial support force using Equation (2).

Bending Experiment

The bending test employed the device illustrated in **Figure 2B**, with preset bending angles of 60°, 90°, and 180°. In this configuration, threads pull opposing sliders inward, inducing bending in the stent graft. Prior to testing, horizontal displacement must be calculated to ensure that the stent bends to the specified angles.

Assuming that the arc length along the outer curve of the stent remains constant during bending, let e_1 be the horizontal displacement and e_2 the vertical displacement of endpoints A and B, α the bending angle, and D_0 the diameter. Based on the geometric diagram in **Figure 4**, the displacements can be derived as follows:

$$e_1 = \frac{l}{2} - \left(\frac{l}{\alpha} - \frac{D_0}{2}\right) * \sin\left(\frac{\alpha}{2}\right) \tag{5}$$

$$e_2 = \left(\frac{l}{\alpha} - \frac{D_0}{2}\right) * (1 - \cos\left(\frac{\alpha}{2}\right)) \tag{6}$$

By substituting the structural parameters of the stent graft and the specified angle α the displacement values for different bending angles can be calculated. **Table 2** lists the values of e_1 and e_2 corresponding to 60°, 90°, and 180° bending.

Before testing, the stent should be pre-bent by 3–5° to prevent axial compression without bending. During the bending process, the threads and the middle plane of the stent must remain coplanar, and thread slippage on pulleys must be avoided to maintain measurement

Table 1. Corresponding relationship between tensile displacement of tensile machine and support diameter

Percentage of compression diameter	D_0/mm	D_n/mm	X/mm
20%	34	27.2	10.68
40%	34	20.4	21.36
60%	34	13.6	32.04

Table 2. The relationship between bending angle and tensile displacement of tensile machine

Stent length/mm	Rotation angle/°	Horizontal displacement e_1/mm	Vertical displacement e_2/mm
130	60	11.18	14.42
130	90	18.15	19.41
130	180	40.12	24.88

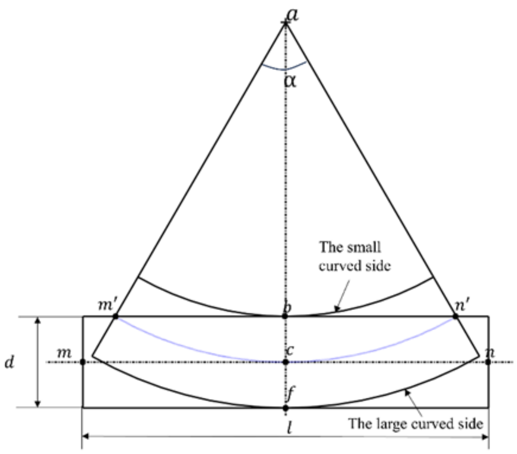

Figure 4. Geometric schematic diagram of stent bending.

accuracy. The tensile testing machine captures and outputs tensile force and thread displacement data in real time. The tensile force is then converted into the spring-back force using Equation (3).

Numerical simulation

The simulation platform uses ABAQUS 2021 for the finite element analysis. To ensure comparability between the simulation and physical experiments, the simulation model is kept consistent with the experimental setup.

The stent material is 316L stainless steel, with a density of 8.03×10^{-8} ton/mm³, a Young's modulus of 200 GPa, and a Poisson's ratio of 0.3. The coating film is made of expanded polytetrafluoroethylene (ePTFE), a medical polymer material, with a density of 2.2×10^{-12} ton/mm³, a Young's modulus of 55.2 MPa, and a Poisson's ratio of 0.46.

Explicit dynamics analysis is employed, with geometric nonlinearity enabled. The time length for the simulation is set to 0.01. The stent ring and coating film are connected by a Tie constraint, with the stent ring as the master surface and the coating film as the slave surface. The stent ring is meshed using eight-node linear hexahedral elements (C3D8R), with reduced integration and hourglass control, and a mesh density of 0.2 mm. The coating film is meshed with four-node curved thin-shell elements, also using reduced integration, hourglass control, and finite membrane strain, with a mesh density of 1 mm.

Simulation verification of radial compression

The thread curve was modeled using SOLIDWORKS 2022. A circular sketch with a diameter of 40.4 mm was created, and a helix was inserted based on the sketch. The helix has a starting angle of 180°, a pitch of 0.2 mm, and one full turn. Truss elements were used to simulate the flexible rope. The thread was meshed with T3D2 elements, and the mesh density was set to 0.5 mm. The thread curve model was imported into ABAQUS CAE 2021, assigned as a truss section, and material properties were set as follows: density 7.98E-09 ton/mm³, Young's modulus 200,000 MPa, Poisson's ratio 0.3.

The simulation is consistent with **Figure 5A**. Axial rotation and rotational degrees of freedom of the stent ring to which the load is applied were constrained, as were the axial and rotational degrees of freedom of the stretching thread. Displacement loads with equal magnitudes and opposite directions were applied at both ends of the thread. The experiment was conducted for compression displacements of 20%, 40%, and 60% of the stent's diameter.

The reaction force in the moving direction of the thread's endpoints during compression was monitored by setting the RF2 history output based on the global coordinate system at the helix endpoints.

Bending simulation verification

Reference points RP1 and RP2 were defined at the centers of the stent graft's two end faces. MPC (Multi-Point Constraint) constraints were applied between the control points and

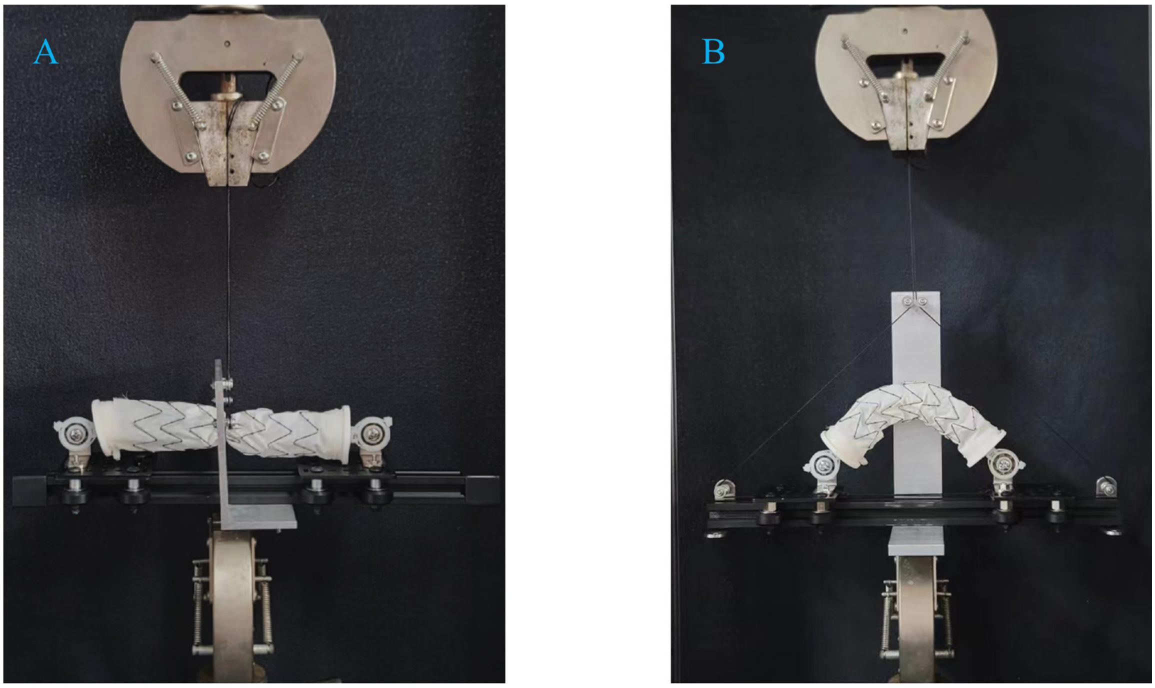

Figure 5. Mechanical performance testing of stent graft. (A) Physical experiment on compression; (B) Physical

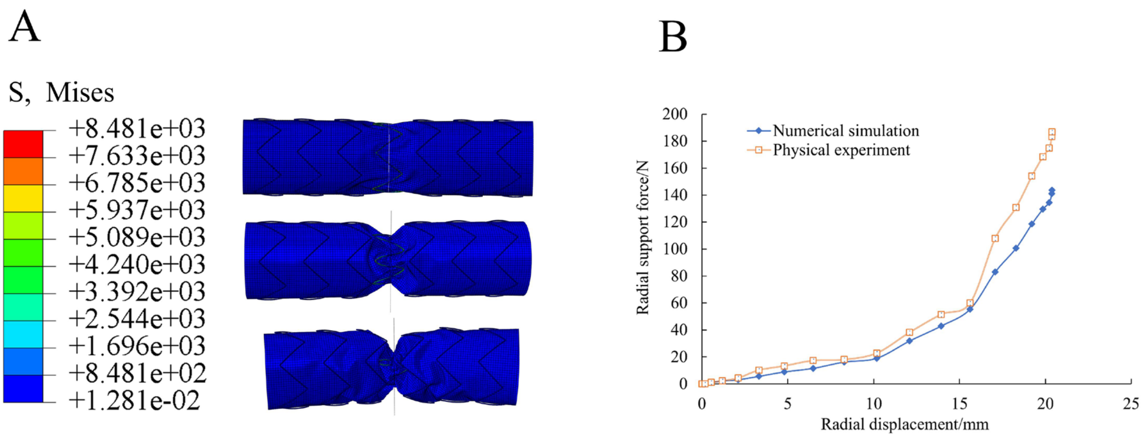

Figure 6. Stress distribution from numerical simulation. (A) Stress nephograms of the stent graft under 20%, 40%, and 60% compression; (B) Stress nephograms of the stent graft bent at 60°, 90°, and 180°.

the nodes at the top of the stent, binding their degrees of freedom together [27]. Equal and opposite angular loads were applied at the two reference points to ensure that the stent reached the desired bending angle. The change in the spring-back force during the bending process was tracked by outputting the reaction forces at the reference points. The simulation is consistent with **Figure 5B**.

III Results

Results of radial compression experiment

The simulation results are shown in **Figure 6**. During the experiment, a specially designed radial loading device, in conjunction with a tensile testing machine, was used to apply a uniform radial displacement load to the stent. The experiment measured the radial support performance of the thoracic aortic stent graft. The results showed the changes in stent morphology and radial support force values under 20%, 40%, and 60% compression displacements, both in physical and simulation experiments.

The simulation results indicate that the radial support force increases gradually with the applied load. The force increases slowly within the 0–15 mm range and rises sharply after 15 mm. In comparison, the physical experiment data largely agree with the finite element simulation results up to 17 mm of compression. However, beyond 17 mm, the increase in radial support force in the physical experiment becomes minimal. On the testing machine's display, the val-

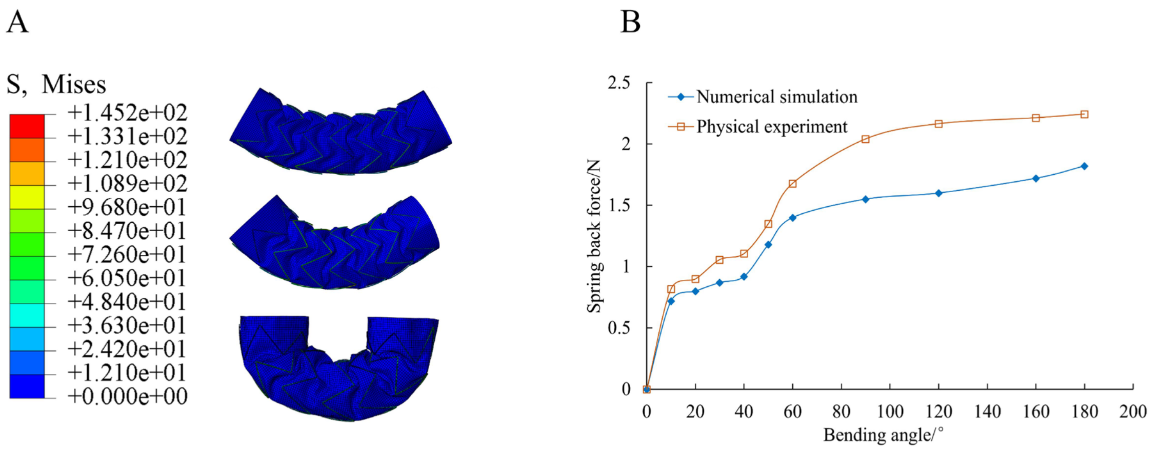

Figure 7. Comparison between Physical Experiment and Numerical Simulation. (A) Curves showing the variation of radial force in the compression experiment and simulation; (B) Curves showing the variation of spring-back force in the physical experiment and the simulation experiment.

ues show only slight fluctuating increases.

Bending experiment results

The simulation results are shown in **Figure 7**. In the physical bending and spring-back force experiment, the stent was placed in the device and bent to angles of 60°, 90°, and 180°. The mechanical parameters of the stent during bending were measured. The experimental results showed that the stent's mechanical performance during bending and recoil was in good agreement with the finite element simulation results.

In the physical experiment, the spring-back force increased rapidly during bending. After reaching 90°, the spring-back force gradually increased. Similarly, in the simulation, the radial support force remained constant when the stent bent within 0–15° but increased rapidly thereafter, showing a trend consistent with the physical experiment.

IV Discussion

The study on the radial support force and bending spring-back force of the thoracic aortic stent graft, conducted through finite element simulations and physical experiments, shows good agreement between the two methods. This consistency effectively validates the effectiveness of the force-measuring device for the thoracic aortic stent graft designed in this study.

The design and construction of the device are straightforward, achieving an effective balance between simplicity and functionality. Core components such as sliders, sliding rails, and pulleys work in coordination, ensuring the stability and reliability of the detection process. The overall structural design meets the required detection standards.

The device's performance test results indicate excellent detection accuracy. When paired with commonly used tensile testing machines, its stability and accuracy surpass those of standard dynamometers. Additionally, repeatability tests show minimal deviations across multiple measurements, demonstrating good stability and ensuring the consistency and reliability of the detection data.

While the results of the two methods align well in most cases, certain discrepancies exist under specific conditions. Notably, in the later stages of stent compression, some stent rings in the physical experiment exhibit yielding behavior, resulting in almost no increase in the radial support force. In contrast, the simulation neglects the stent material's plastic behavior, as yield stress and hardening modulus are not incorporated, which keeps the stent in the elastic phase during compression. Additionally, as the compression diameter increases, self-contact behavior occurs in the stent rings, causing the radial support force curve to become steeper in the simulation.

To improve the accuracy of future research, the following improvements are recommended: first, use a different thread material to reduce friction; second, optimize the finite element simulation model to more precisely account for the nonlinear material characteristics and complex boundary conditions; third, increase the number of experimental samples to minimize the impact of individual variations on the results.

V Conclusions

This study developed a mechanical property testing device for large-vessel stents, which can be used in conjunction with a tensile testing machine. The device is capable of performing mechanical property tests on radial support force and bending spring-back force. Physical experiments were conducted to test the support and compliance properties of the self-designed 5-peak gradient stent grafts. The results demonstrated that the stents have good support and excellent compliance, and the corresponding mechanical properties were identified. Finite element simulations were used to model the radial compression and bending of the stent grafts, and the corresponding mechanical change curves were obtained. These curves were consistent with the physical experiment results, which further validated the reliability of the stent graft testing device designed in this study.

Author contributions: Ailing Zhang conceived the project and formulated the overall experimental plan. Yu Zhou was responsible for the general assembly of the device, conducting the experiments, and processing the data. Shiju Yan completed the design of the device. The manuscript was jointly completed by all the authors.

References

[1] Dake MD, Kato N, Mitchell RS, et al. Endovascular stent-graft placement for the treatment of acute aortic dissection. N Engl J Med 1999;340(20):1546-1552.

[2] Perrin D, Demanget N, Badel P, et al. Deployment of stent grafts in curved aneurysmal arteries: toward a predictive numerical tool. Int J Numer Method Biomed Eng 2015;31(1):e02698.

[3] Kumar A, Bhatnagar N. Finite element simulation and testing of cobalt-chromium stent: a parametric study on radial strength, recoil, foreshortening, and dogboning. Comput Methods Biomech Biomed Engin 2021;24(3):245-259.

[4] Pan C, Han Y, Lu J. Structural Design of Vascular Stents: A Review. Micromachines (Basel) 2021;12(7):770.

[5] Matsumoto T, Matsubara Y, Aoyagi Y, et al. Radial force measurement of endovascular stents: Influence of stent design and diameter. Vascular 2016;24(2):171-176.

[6] Li Z, Kleinstreuer C. Analysis of biomechanical factors affecting stent-graft migration in an abdominal aortic aneurysm model. J Biomech 2006;39(12):2264-2273.

[7] Aras T, Tayeh M, Aswad A, et al. Exploring Type IIIb Endoleaks: A Literature Review to Identify Possible Physical Mechanisms and Implications. J Clin Med 2024;13(15):4293.

[8] Dong Z, Fu W, Wang Y, et al. Stent graft-induced new entry after endovascular repair for Stanford type B aortic dissection. J Vasc Surg 2010;52(6):1450-1457.

[9] Shahbazian N, Romero DA, Forbes TL, et al. Identification of geometric and mechanical factors predictive of bird-beak configuration in thoracic endovascular aortic repair using computational models of stent graft deployment. JVS Vasc Sci 2022;3:259-273.

[10] Li M, Ma T, Cai Y, et al. Numerical simulation of the distal stent graft-induced new entry after TEVAR. Int J Numer Method Biomed Eng 2024;40(5):e3819.

[11] Joo HC, Youn YN, Ko YG, et al. Comparison of open surgical versus hybrid endovascular repair for descending thoracic aortic aneurysms with distal arch involvement. J Thorac Dis 2018;10(6):3548-3557.

[12] Tang F, Hu C, Huang S, et al. An Innovative Customized Stent Graft Manufacture System Assisted by Three-Dimensional Printing Technology. Ann Thorac Surg 2021;112(1):308-314.

[13] Ryu DS, Won DS, Kim JW, et al. Efficacy of thermoplastic polyurethane and gelatin blended nanofibers covered stent graft in the porcine iliac artery. Sci Rep 2022;12(1):16524.

[14] Vellaparambil R, Han WS, Di Giovanni P, et al. Potential of auxetic designs in endovascular aortic repair: A computational study of their mechanical performance. J Mech Behav Biomed Mater 2023;138:105644.

[15] Schmidt W, Behrens P, Brandt-Wunderlich C, et al. In vitro performance investigation of bioresorbable scaffolds - Standard tests for vascular stents and beyond. Cardiovasc Revasc Med 2016;17(6):375-383.

[16] Barragan P, Garitey V, Mouneimne K, et al. Longitudinal compression behaviour of coronary stents: a bench-top comparative study. EuroIntervention 2014;9(12):1454-1462.

[17] Xue W, Lin J, Wang F, et al. Design and mechanical behaviors of sutureless prototype composite nitinol stent-grafts. Text Res J 2018;88(13):1517-1530.

[18] Zhuravleva IY, Timchenko TP, Vladimirov SV, et al. Ab ovo: Factors Affecting the Radial Stiffness of Thoracic Aorta Stent-Grafts. Sovrem Tekhnologii Med 2021;13(1):17-25.

[19] Maleckis K, Deegan P, Poulson W, et al. Comparison of femoropopliteal artery stents under axial and radial compression, axial tension, bending, and torsion deformations. J Mech Behav Biomed Mater 2017;75:160-

168.
[20] Kwiecinski J, Cheng CP, Uberoi R, et al. Thoracic aortic parallel stent-graft behaviour when subjected to radial loading. J Mech Behav Biomed Mater 2021;118:104407.
[21] Voûte MT, Hendriks JM, van Laanen JH, et al. Radial force measurements in carotid stents: influence of stent design and length of the lesion. J Vasc Interv Radiol 2011;22(5):661-666.
[22] Ormiston JA, Dixon SR, Webster MW, et al. Stent longitudinal flexibility: a comparison of 13 stent designs before and after balloon expansion. Catheter Cardiovasc Interv 2000;50(1):120-124.
[23] Demanget N, Latil P, Orgéas L, et al. Severe bending of two aortic stent-grafts: an experimental and numerical mechanical analysis. Ann Biomed Eng 2012;40(12):2674-2686.
[24] Yan S, Song C, Yang Y, et al. Design and implementation of mechanical property testing equipment for thoracic aortic stent grafts. Minim Invasive Ther Allied Technol 2024;33(2):120-128.
[25] Yan S, Song C, Si Y, et al. Design of non-equal-strut stent hoops for structural optimization of thoracic aortic stent-grafts. Minim Invasive Ther Allied Technol 2022;31(1):58-71.
[26] Zhang L, Chen X, Liu M. Research of Customized Aortic Stent Graft Manufacture. IOP Conf Ser: Mater Sci Eng 2017;187(1):012027.
[27] Vellaparambil R, Han WS, Di Giovanni P, et al. Computational Comparison of the Mechanical Behavior of Aortic Stent-Grafts Derived from Auxetic Unit Cells. Cardiovasc Eng Technol 2024;15(2):199-210.